An Optimal Beamforming Algorithm for Phased-Array Antennas Used in Multi-Beam Spaceborne Radiometers

An Optimal Beamforming Algorithm for Phased-Array Antennas Used in Multi-Beam Spaceborne Radiometers

O. A. Iupikov[1], M. V. Ivashina[1], K. Pontoppidan[2], P. H. Nielsen[2], C. Cappellin[2], N. Skou[3], S. S. Søbjærg[3], A. Ihle[4], D. Hartmann[4], K. v. 't Klooster[5]

[1]Signals and Systems Department of the Chalmers University of Technology, Gothenburg, Sweden, e-mail: oleg.iupikov@chalmers.se, marianna.ivashina@chalmers.se

[2]TICRA, Copenhagen, Denmark, e-mail: cc@ticra.com, kp@ticra.com, phn@ticra.com

[3] DTU-Space, Technical University of Denmark, Kgs. Lyngby, Denmark, e-mail: ns@space.dtu.dk, sss@space.dtu.dk

[4] HPS GmbH, Munich, Germany, e-mail: ihle@hps-gmbh.com, hartmann@hps-gmbh.com

[5]European Space Research and Technology Centre, Noordwijk, The Netherlands, e-mail: Kees.van.t.Klooster@esa.int

***Abstract*—Strict requirements for future spaceborne ocean missions using multi-beam radiometers call for new antenna technologies, such as digital beamforming phased arrays. In this paper, we present an optimal beamforming algorithm for phased-array antenna systems designed to operate as focal plane arrays (FPA) in push-broom radiometers. This algorithm is formulated as an optimization procedure that maximizes the beam efficiency, while minimizing the side-lobe and cross-polarization power in the area of Earth, subject to a constraint on the beamformer dynamic range. The proposed algorithm is applied to a FPA feeding a torus reflector antenna (designed under the contract with the European Space Agency) and tested for multiple beams. The results demonstrate an improved performance in terms of the optimized beam characteristics, yielding much higher spatial and radiometric resolution as well as much closer distance to coast, as compared to the present-day systems.**

***Index Terms*—radiometer, reflector antenna, phase array feed.**

I. Introduction

Recent advances in phased-array antenna technologies and low-cost active electronic components open up new possibilities for designing Earth observation instruments. One example of such technologies is digital beamforming phased-array feeds (PAFs) (often referred to as dense focal plane arrays [1]). Using PAFs is especially attractive in spaceborne radiometers in so-called push-broom configuration [2], where a large number of beams cover a wide region (swath) of the Earth simultaneously to achieve high sensitivity. For such radiometers, various optics concepts have been investigated [3], and the optimum solution has been found to be an offset toroidal single reflector antenna. This reflector structure is rotationally symmetric around its vertical axis, and thus is able to cover a wide swath range. However, its aperture field exhibits significant phase errors due to the non-ideal (parabolic) surface of the reflector that lead to the beam deformation. Accurate compensation for these effects requires the use of a moon-shaped PAF (as shown on fig.1) as well as dedicated beamforming algorithms. Development of such an optimal algorithm is the objective of this paper.

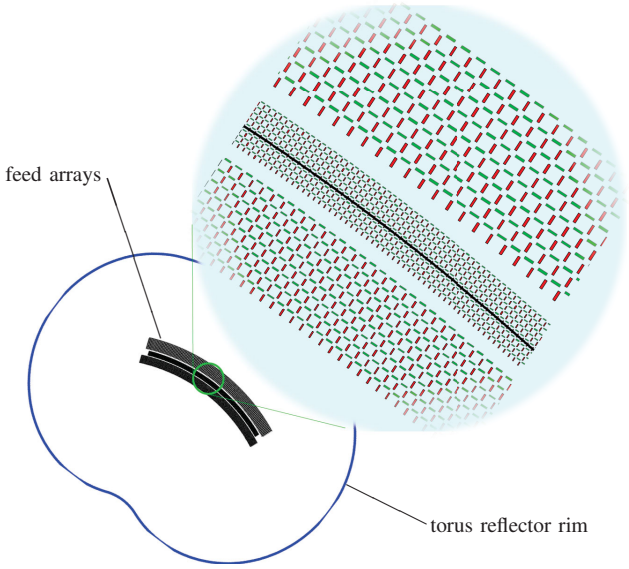

Fig. 1. A schematic layout of the moon-shaped phased-array feeds for X-, Ku- and C-bands that are located in the focal field region of the torus reflector. The arrays comprise dual-polarized dipole antenna elements, denoted by the red and green lines. The black curve denotes the focal arc of the torus reflector.

II. Array design

An initial design of the PAF has been reported in [4]; where the array elements are arranged on the rectangular grid. For the current study, we have re-arranged the element positions along the focal-field arc of the torus reflector (see Fig. 1). This re-arrangement has led to the moon-shaped layout of the present PAF enabling similar focal-field distributions that are resulted from different incident directions upon the apertures of the corresponding sub-arrays. Thanks to this advantageous property, optimization of the beamformer weights for multiple beams reduces to the optimization of a single set of weights for one beam only, and most importantly, to the virtually identical beam shapes over the wide observation range. Furthermore, the

new design consists of dual-polarized 0.5λ-dipole antennas, having higher polarization purity, as compared to the tapered-slot antenna elements used in the array in [4].

To simplify the modeling of the array for this study, we have made the following assumptions: (i) all array elements have the same radiation patterns; (ii) no mutual coupling and edge truncation effects are accounted for the array, and; (iii) the dipoles are located above an infinite ground plane. In the future studies, these simplifications will be eliminated.

III. Optimal Beamforming Algorithm

A. Generic formulation

The proposed optimization algorithm is formulated as the maximum Signal-To-Noise beamformer (MaxSNR) [5], where the antenna efficiency - defined for a given direction of observation corresponding to the beam center - is maximized, while minimizing the power received from the other directions. The weight vector for this beamformer can be written as

$$\mathbf{w}_{\text{MaxSNR}} = \mathbf{C}^{-1}\mathbf{e}, \text{ with SNR} = \mathbf{e}^{H}\mathbf{w}_{\text{MaxSNR}}, \qquad (1)$$

where the vector $\mathbf{e} = [e_1, \ldots, e_N]^T$ holds the signal-wave amplitudes at the receiver outputs and arises due to an externally applied electromagnetic plane wave $\boldsymbol{E}_{\text{i}}$; and $\mathbf{C}$ is a Hermitian spectral noise-wave correlation matrix holding the correlation coefficients between the outputs of the array receiving system.

If we assume a noiseless receiver system, the matrix $\mathbf{C}$ represents the antenna noise correlation matrix, which contains the noise correlation coefficients due to external noise sources (that are present in the region of observation on the Earth as well as outside). The elements of $\mathbf{C}$ can be calculated through the pattern-overlap integrals between $\boldsymbol{f}_n(\Omega)$ and $\boldsymbol{f}_m(\Omega)$, which are the nth and mth embedded element pattern (EEP) of the array (defined after the reflection from the dish), respectively [6], i.e.,

$$C_{mn} = \int T_{\text{ext}}(\Omega)[\boldsymbol{f}_m(\Omega) \cdot \boldsymbol{f}_n^*(\Omega)]\, \mathrm{d}\Omega, \qquad (2)$$

where $T_{\text{ext}}(\Omega)$ is the brightness temperature distribution of the environment. To meet the radiometer requirements [2], the function $T_{\text{ext}}(\Omega)$ is chosen such that it has low temperature values in the region of the expected main lobe (down to -20 dB level) and high values outside of this region. In this way, we realize the maximization of the beam efficiency – defined at the -20 dB level – while minimizing the side-lobe and cross-polarization power outside of this region, as required for the radiometers.

B. Computation acceleration

When constructing matrix $\mathbf{C}$, one should realize that its filling can be an extremely time-consuming procedure as it requires computation of all secondary EEPs over the entire sphere and evaluation of the pattern overlap integral (2) for all combinations of EEPs (see Tabl. I). In order to speed-up the computational process, we have therefore represented the matrix $\mathbf{C}$ as a sum of two contributions, matrices $\mathbf{C}_1$ and $\mathbf{C}_2$ that can be calculated relatively fast. The first matrix is obtained by using the secondary EEPs computed in a limited angular range around the main lobe region, while the second matrix is used for correcting for the spillover effects and evaluated through the primary feed patterns. The brightness temperature distribution functions $T_{\text{ext}}(\Omega)$ corresponding to $\mathbf{C}_1$ and $\mathbf{C}_2$ are illustratively shown in the insets of Fig. 2.

The table below cross-compares the computational time at Ku band that is needed for the simulations (using GRASP) of the secondary patterns over the entire sphere (when computing the matrix $\mathbf{C}$ through the brute-force approach) and over the reduced region with the post-correction for the spillover effect (when computing the matrices $\mathbf{C}_1$ and $\mathbf{C}_2$ through the proposed approach). There is obvious advantage in using the latter approach, especially for the systems with a large number of beams and high operational frequencies.

TABLE I
Computational time of the matrix $\mathbf{C}$ at Ku-band (18.7 GHz)

Brute-force approach		**Proposed approach**	
Computing sec. EEPs	Computing $\mathbf{C}$	Computing sec. EEPs	Computing $\mathbf{C}_1$ and $\mathbf{C}_2$
$\sim$ 9 months	*no data*	3 hours	5 min/beam

C. Iterative procedure for constraints on the dynamic range of the weights

The proposed beamformer, as described in sub-section III.A, has been extended so as to include constraints on the dynamic range of the weights that should not exceed a certain value. For this purpose, we have implemented an iterative procedure that modifies the reference weighting coefficients (as determined by the MaxSNR beamformer), while aiming to maintain the shape of the PAF pattern as close as possible to the reference one. This ensures that the radiometer parameters are as similar as possible to those obtained with the reference set of weights. The corresponding algorithm is listed as follows:

- At the first iteration ($q = 1$) the reference weight vector $\mathbf{w}^{(1)}$ is calculated using (1) with the initial noise-wave

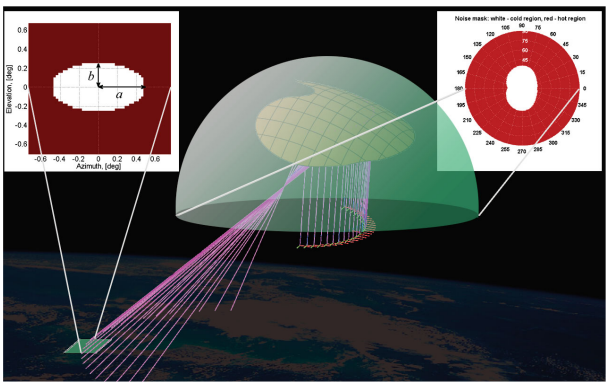

Fig. 2. The T_{ext} mask-constrained functions defined for the calculation of the antenna noise correlation matrices $\mathbf{C}_1$ due to the noise sources in the Earth region (see the inset in the left upper corner) and $\mathbf{C}_2$ due to the noise sources in the sky region (see the inset in the right upper corner). The toroidal reflector fed with a PAF is in the middle of the illustration, where the multiple beams point to the Earth.

correlation matrix $\mathbf{C}^{(1)}$.

- At iteration $q = 2, 3\ldots$ a new weight vector $\mathbf{w}^{(q)}$ is computed using the noise covariance matrix $\mathbf{C}^{(q)}$, diagonal elements of which are a function of the weight vector $\mathbf{w}^{(q-1)}$ obtained after the previous iteration, i.e.,

$$C_{nn}^{(q)} = C_{nn}^{(q-1)} f(|w_n^{(q-1)}|) \tag{3}$$

where f is a receiver function that needs to be provided as an input to the algorithm; it should have such a behaviour that the lower the weight of the array antenna element, the higher the function value is (which physically corresponds to an increase in the noise temperature of the corresponding receiver channel). In the numerical results presented hereafter, a filter function is used whose values are close to zero when the weights magnitude $|w_i|$ are higher than w_{constr}, and which has a sharp linear increase near w_{constr}. In this way, f is similar to the inverse step function near w_{constr} (Fig. 3). Here, w_{constr} is the value of the amplitude weight constraint, which is typically in the order of -30 dB or -40 dB.

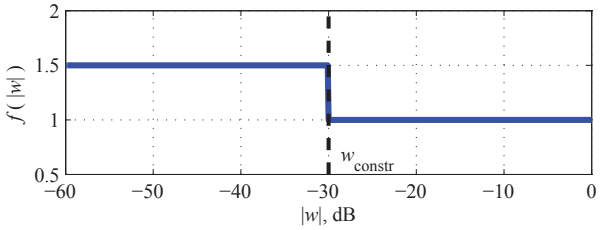

Fig. 3. The function f used in the iterative procedure described in section III.C.

- Check whether all the weights are higher than w_{constr}, or negligibly low (i.e. -80 dB in this work). If this condition is satisfied, the iterative procedure is terminated. The channels with negligible weights are switched-off, while the resulting set of weight coefficients is considered to be the final one.

In order to use the beamformer for scanned beams, the noise temperature distribution function $T_{\text{ext}}(\Omega)$ must be provided for each of them and the matrix $\mathbf{C}$ needs to be recomputed.

More detailed on the formulation and implementation of the beamformer can be found in [7].

IV. Parametric Studies

A. Beamformer

The proposed beamformer has two parameters for defining the "cold" ellipse of the mask-constrained function $T_{\text{ext}}(\Omega)$ that are used for the computation of $\mathbf{C}_1$: the ellipse major semi-axis a and the axis ratio a/b (see Fig. 2, top-left inset). Since the area of the ellipse is related to the area of the main lobe over which the received power is maximized, and the size of the foot print is known from specifications, the range of practical values for a and the axis ratio a/b is relatively small, and hence the parametric study to find the optimal values is not time-consuming.

The considered radiometer characteristics [2] as functions of these parameters have been computed and the most critical ones, i.e. the distance-to-land and footprint size, are shown in Fig. 4. As a trade-off between the required values of the distance-to-land (< 15 km) and the footprint size (< 10 km), the following best values have been chosen: $a = 0.535$ and $a/b = 1.3$.

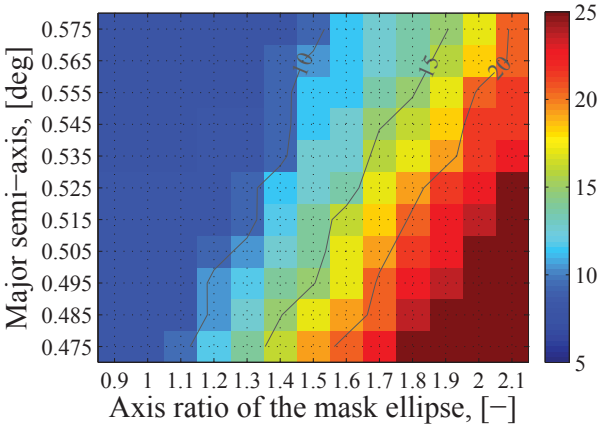

(a)

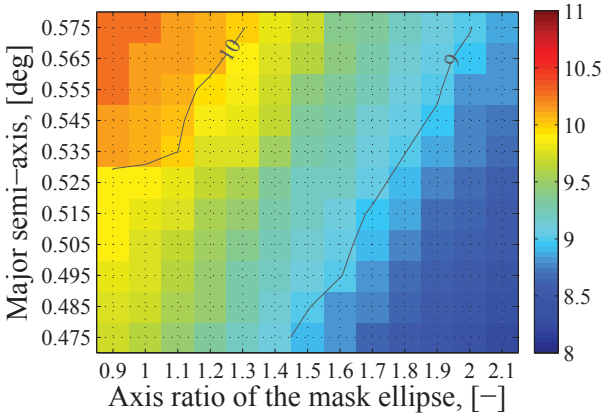

(b)

Fig. 4. (a) Distance-to-land, [km]; and, (b) footprint size, [km], as functions of a and a/b used for the definition of the mask-constrained function $T_{\text{ext}}(\Omega)$ as shown on Fig. 2.

B. PAF size and final radiometer characteristics

For the beamformer with the parameters as obtained above, we have studied a range of PAF designs which have a number of rows varying from 5 to 8. The computed radiometer characteristics for the range of rows are shown in Fig. 5. As one can see, to satisfy all radiometer requirements, the minimum number of rows in the PAF must be equal to 6.

The optimized set of weight coefficients are shown in Fig. 6. The corresponding pattern of the phased-array feed and the pattern of the entire reflector antenna system for the on-axis beam are shown in Fig. 7. We can observe the very fine shape of the illumination pattern across the reflector aperture, and well-behaved final beam with the minimized side-lobe levels.

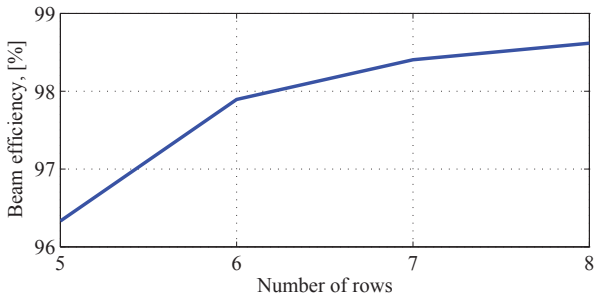

(a)

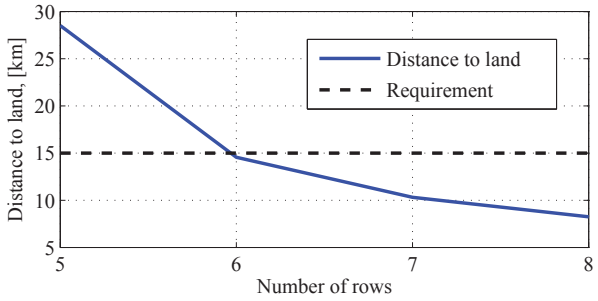

(b)

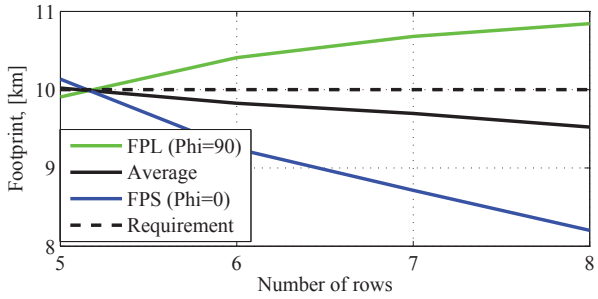

(c)

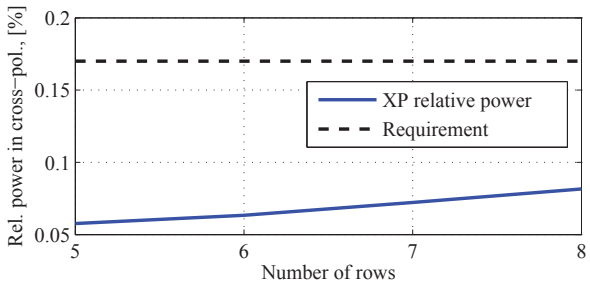

(d)

Fig. 5. Radiometer characteristics, including the beam efficiency, distance to land, footprint and relative cross-polarization power, vs. the number of rows in the PAF.

The levels of the side lobes are different, though, over the angular region; that results in the angular dependence of the distance-to-land parameter, which becomes a function of the coast line position. Since the footprint on the Earth resulted from this beam, is not symmetric either, we have investigated whether the distance-to-land requirement is satisfied for all possible locations on the land line with respect to the beam

TABLE II
FINAL RADIOMETER CHARACTERISTICS AT KU-BAND (18.7 GHZ)

Radiometer characteristic	**Requirement**	**Gaussian feed**	**PAF** $6 \times 19 \times 2$ **elem.** $d_{\text{el}} = 0.75\lambda$
Beam efficiency [%]		73.9	97.9
XP-power, [%]	0.34	0.38	0.06
Dist. to land, [km]	15	90.8	14.6
Beam width, [deg]		0.38	0.357
Footprint (FP), [km]	10	10.5	9.8
FP ellipticity		1.13	1.12

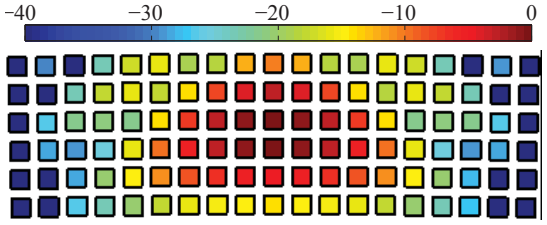

Fig. 6. The array element amplitude weight coefficients, [dB], as obtained with the proposed beamforming algorithm. Each block represents an element of the array.

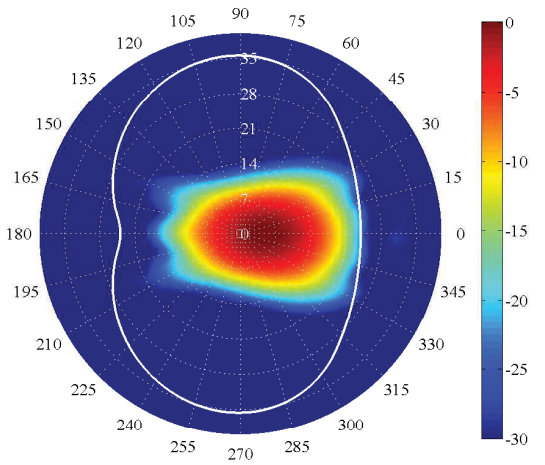

(a)

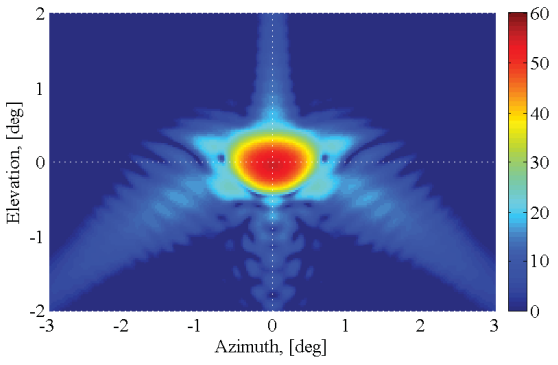

(b)

Fig. 7. (a) The optimized pattern of the PAF when illuminating the aperture of the torus reflector, [dB], and (b) the corresponding final beam of the entire reflector antenna system for the case of the center beam, [dBi].

footprint. As the data on Fig. 8 show, the PAF with 6 rows satisfies this criterion for all possible positions.

The corresponding radiometer characteristics for the on-axis beam are summarized in Table II. Thanks to the rotational symmetry of the reflector and the moon-shaped array layout, the scanned beams will have similar characteristics.

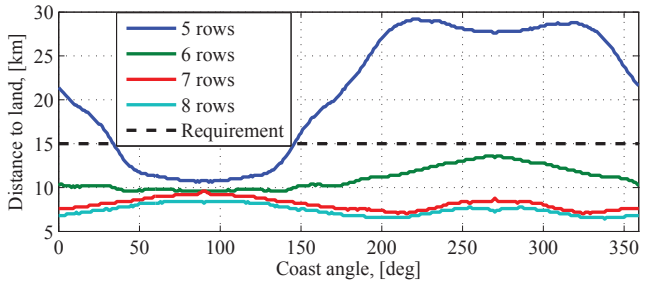

Fig. 8. Distance-to-land as a function of angle at which the coast line is approached by the beam for different array sizes.

V. Conclusion

An optimal beamforming algorithm for phased-array antennas, such as considered for the next generation multi-beam radiometers, has been presented and evaluated for a currently designed prototype system. It yields well behaved multiple beams which satisfy strick requirements to the footprint on the Earth, minimized power in the side-lobes and cross-polarization as well as the distance-to-coast. The proposed algorithm is formulated in a closed form and enables different performance trade-offs.

References

[1] M. Ivashina and J. Bregman, "A way to improve the field of view of the radiotelescope with a dense focal plane array," in *Proc. of the Int. conf. on Microwave and Telecommunication Technology*, Sevastopol, Ukraine, Sep. 2002.

[2] C. Cappellin, K. Pontoppidan, P. Nielsen, N. Skou, S. S. Søbjærg, A. Ihle, D. Hartmann, M. Ivashina, O.Iupikov, and K. v. t Klooster, "Novel multi-beam radiometers for accurate ocean surveillance," in *Proc. European Conference on Antennas and Propag. (EuCAP)*, The Hague, The Netherlands, Apr. 2014, pp. 1–4.

[3] P. Nielsen, K. Pontoppidan, J. Heeboell, and B. L. Stradic, "Design, manufacture and test of a pushbroom radiometer," in *Antennas and Propagation, 1989. ICAP 89., Sixth International Conference on (Conf. Publ. No.301)*, Coventry, United Kingdom, Apr. 1989, pp. 126–130.

[4] O. A. Iupikov, M. V. Ivashina, K. Pontoppidan, P. H. Nielsen, C. Cappellin, N. Skou, S. S. Søbjærg, A. Ihle, D. Hartmann, and K. v. 't Klooster, "Dense focal plane arrays for pushbroom satellite radiometers," in *Proc. European Conference on Antennas and Propag. (EuCAP)*, Hague, The Netherlands, Apr. 2014, pp. 1–5.

[5] H. L. van Trees, *Optimum Array Processing – Part IV of Detection, Estimation, and Modulation Theory*. New York: Wiley, 2002.

[6] M. V. Ivashina, O. Iupikov, R. Maaskant, W. A. van Cappellen, and T. Oosterloo, "An optimal beamforming strategy for wide-field surveys with phased-array-fed reflector antennas," *IEEE Trans. Antennas Propag.*, vol. 59, no. 6, pp. 1864–1875, Jun. 2011.

[7] O. Iupikov, "Phased-array-fed reflector antenna systems for radio astronomy and Earth observations," Licentiate Thesis, Institutionen för signaler och system, Antenner, Chalmers tekniska högskola, Göteborg, Oct. 2014.